Fractionation of reward processing into independent neural representations by novel decoding principle

Tianye Jia (tianyejia@fudan.edu.cn)
Fudan University https://orcid.org/0000-0001-5399-2953
Shitong Xiang
Fudan University
Chao Xie
Institute of Science and Technology for Brain-Inspired Intelligence, Fudan University, Shanghai, China
Zhichao Zhu
Fudan University
Jujiao Kang
Fudan University
Wei Cheng
Fudan University
Gunter Schumann
Centre for Population Neuroscience and Precision Medicine (PONS) and SGDP Centre, Institute of Psychiatry, Psychology and Neuroscience, King's College London, London SE5 8AF, United Kingdom
https://orcid.org/0000-0002-7740-6469
Trevor Robbins
University of Cambridge https://orcid.org/0000-0003-0642-5977
Jianfeng Feng
Department of Computer Science, University of Warwick

Technical Report

Keywords:

Posted Date: April 6th, 2022

DOI: https://doi.org/10.21203/rs.3.rs-845993/v1

Title: Fractionation of reward processing into independent neural representations by novel decoding principle

Authors: Shitong Xiang[1,2†], Tianye Jia[1,2,3,4†*], Chao Xie[1,2†], Zhichao Zhu[1,2], Jujiao Kang[1,2,7], Wei Cheng[1,2], Gunter Schumann[4,5], Trevor W. Robbins[1,2,6*], Jianfeng Feng[1,2,7,8,9*]

Affiliations:

[1] Institute of Science and Technology for Brain-Inspired Intelligence, Fudan University, Shanghai, China.
[2] Key Laboratory of Computational Neuroscience and Brain-Inspired Intelligence (Fudan University), Ministry of Education, China;
[3] Centre for Population Neuroscience and Precision Medicine (PONS), Institute of Psychiatry, Psychology & Neuroscience, SGDP Centre, King's College London, United Kingdom, SE5 8AF;
[4] Centre for Population Neuroscience and Precision Medicine (PONS), Institute of Science and Technology for Brain-Inspired Intelligence, Fudan University, Shanghai, China.
[5] Centre for Population Neuroscience and Precision Medicine (PONS), Dept. of Psychiatry and Psychotherapy, CCM, Charite Universitaetsmedizin, Berlin, Germany.
[6] Department of Psychology and Behavioural and Clinical Neuroscience Institute, University of Cambridge, Cambridge, United Kingdom;
[7] Shanghai Center for Mathematical Sciences, Fudan University, Shanghai, China;
[8] Department of Computer Science, University of Warwick, Coventry, United Kingdom;
[9] School of Mathematical Sciences and Centre for Computational Systems Biology, Fudan University, Shanghai, China.

† These authors contributed equally to this work.

* Correspondence authors.

Jianfeng Feng (Address: Institute of Science and Technology for Brain-inspired Intelligence, Fudan University, Shanghai, 200433, China. Email: jianfeng64@gmail.com)

or

Tianye Jia (Address: Institute of Science and Technology for Brain-inspired Intelligence, Fudan University, Shanghai, 200433, China. Email: tianyejia@fudan.edu.cn)

or

Trevor W. Robbins (Address: Department of Psychology and Behavioural and Clinical Neuroscience Institute, University of Cambridge, Cambridge, United Kingdom. Email: twr2@cam.ac.uk)

Abstract:

How to retrieve latent neurobehavioural processes from complex human neurobiological signals is an important yet unresolved challenge. Processing value and salience information are fundamental yet mutually confounded pathways of reward reinforcement. Here, we develop a novel analytical approach, orthogonal-Decoding multi-Cognitive Processes (DeCoP), to decode brain-wide responses into spatially overlapping, yet functionally independent, evaluation and readiness networks during the anticipation of reward or punishment. Our findings indicate that this functional independence is modulated differentially by those neural systems innervated by the cortico-mesolimbic and nigro-striatal dopamine projections. The segregation of evaluation and readiness neural responses from a unified input signal was also achievable using a theoretical neuronal population-coding model, hence further advancing our understanding of the neural basis involved in motivational processing. Furthermore, our novel theoretical approach could potentially be applied more generally to decode multiple latent neurobehavioral processes and thus advance both the design and hypothesis testing in cognitive task paradigms.

Main

The brain frequently engages parallel processing involving different latent behavioural processes mediated by functionally distinct, though spatially overlapping, neural networks [1]. Previously, human functional neuroimaging studies have had difficulty in unravelling these processes from basal compound physiological signals [2-4], which has made it difficult to build process-specific and mechanistic models of the brain [5].

Reward/punishment processing is perhaps the most adaptive function of the behavioural control system, optimising outcomes through both positive and negative reinforcement [6]. Recent overarching frameworks propose two different cognitive processes engaged in parallel during rewarded or punished behaviour, namely evaluation (i.e. scaling signal values from reward to punishment) and response readiness (subsuming arousal and attentional salience, contributing to response preparatory processes) [6, 7]. The evaluation process is essential for guiding upcoming action selections based on their value, for which the brain has evolved dedicated regions/circuits [8-13]. Complementary to evaluation, both reward and punishment, as highly salient events, attract greater attention than neutral stimuli, also engaging greater levels of motor preparation and emotional arousal [14-16], hence contributing to response (including motor) readiness. Therefore, evaluation and readiness signals are inevitably confounded with each other during reward/punishment processing. Unfortunately, decomposing this compound signal, for example in human fMRI studies, has proven challenging because these two components cannot be identified by using only reward (or only punishment) stimuli in many experimental paradigms. Previous attempts have been made to overcome this problem through identifying spatially dissociated brain regions specific for either evaluation or readiness [2, 3, 17]. However, these approaches have failed to disentangle signals in brain regions known to encode both evaluation and readiness signals, for example, in the striatum and the ventromedial prefrontal cortex (vmPFC) [7, 16, 18]. Further, the existing studies have not provided convincing evidence to clarify the neural basis for the assumption of functional independence of the evaluation and readiness processes.

In the present study, through an innovative approach, we have achieved a brain-wide voxel-wise decomposition of process-specific neurobiological representations of complex neurobehavioural processes for the first time. By implementing this method, we identified two functionally independent yet spatially overlapping neural networks that process evaluation and readiness signals, implicating distinct dopaminergic pathways from VTA and SNc, respectively. We further demonstrated that most brain regions only encoded the relative rank of the signal stimuli, except for the dACC and insula, which coded precise input signals. Finally, based on these results, we established an integrated neural network model that could encode the value-related stimuli (i.e. monotonically from punishment through neutral to reward) into two separate outputs of value and salience signals, hence further advancing our understanding of the neural mechanisms involved in reward/punishment processing.

Experiment design and behaviour outcomes

A monetary incentive delay (MID) task (Fig. 1a), one of the classical and widely used fMRI paradigms for reward processing, was conducted in 1939 children aged 9-10 from the ABCD study [19] (Extended Data Table. 1) to assess reward/punishment processing with gain/loss conditions for small or large amounts of money and a neutral condition (i.e., -5.0 $, -0.2 $, 0, 0.2 $ or 5.0 $). Briefly, cues are shown to indicate the trial condition as well as the amount of money involved at the anticipation phase. Participants are then shown a target stimulus and asked to respond to gain reward or avoid loss after a jittered anticipatory delay.

Overall, participants demonstrated better task performance in responding to both reward and punishment stimuli (Accuracy: Reward vs Neutral, $t_{1,927}$ = 38.96, p < 1E-245, Punishment vs Neutral, $t_{1,927}$ = 29.41, p < 1E-156; Reaction Time: Reward vs Neutral, $t_{1,927}$ = -10.98, p < 1E-26, Punishment vs Neutral, $t_{1,927}$ = -9.69, p < 1E-20; Fig. 1b). Further, using a monotonic contrast [-2, -1, 0, 1, 2] to represent the step-wise increment of signal values and a corresponding V-shaped contrast [2, 1, 0, 1, 2] to represent the salience effect of input at each condition (i.e. the absolute value of signals) (Fig. 1c), we estimated the contributions of both contrasts to task performance through

a general linear model at the individual level, and found both higher accuracy and faster reaction times were strongly associated with a higher salience effect (Accuracy: $t_{1,927}$ = 42.74, p < 1E-281; Reaction Time: $t_{1,927}$ = -14.23, p < 1E-43) but not with the signal value itself, i.e. no difference between reward and punishment trials (Accuracy: $t_{1,927}$ = 1.87 p = 0.06; Reaction Time: $t_{1,927}$ = -1.63 p = 0.11). Such a hugely differentiated result hence implied that our brain may have different dedicated neural circuits underlying the processes of value and salience signals.

Decomposed neural representations

We next introduced a novel approach, the orthogonal-Decoding of multi-Cognitive Processes (DeCoP), to identify the neural representation of evaluation and readiness encoding in the anticipation phase. The central idea is to note that there are five experimental conditions that can evoke condition-specific neuronal responses. This means that there exists four orthogonal contrasts or patterns of responses over the five conditions (i.e., number of conditions minus one for the constant term). Crucially, these orthogonal contrasts should have a clear interpretation, by design, in terms of latent neurobehavioural processes. For instance, in the second-level analyses of BOLD signals, we again implemented the two plausible contrasts evulation (i.e., [-2, -1, 0, 1, 2]) and readiness (i.e., [2, 1, 0, 1, 2]) that respectively reflected putative independent hypothetical processes of value and salience information across five task conditions. It should be noted that not only are both evaluation and readiness contrasts orthogonal to each other (i.e. their covariance equals 0), but their complementary orthogonal contrasts (i.e., the N-shape model: [-1, 2, 0, -2, 1] and the W-shape model: [1, -2, 2, -2, 1]) were also available and could explain information not accounted for by the hypothetical contrasts for evaluation and readiness (Fig. 2a). We were thus able to retrieve the decomposed signal components of those underlying confounded processes and assess the significance of their respective (and collective) expression over the entire brain. (Extended Data Fig. 1a, see Methods for more details). In our initial report of the results, we will focus on evaluation and readiness components and then place them in the larger context of a four-dimensional space of reward processing in the human brain.

Notably, the vmPFC (Brodmann area [BA] 10-11; Peak MNI: [-9, 49, -9], $t_{1,927}$ = 15.69, Cohen's D = 0.36; Cluster: 615 voxels, $p_{\text{FWE-corr}}$ = 1.87E-08) and ventral striatum (VS, Peak MNI: [-7, 25, -3], $t_{1,927}$ = 14.21, Cohen's D = 0.32; Cluster: 634 voxels, $p_{\text{FWE-corr}}$ = 1.36E-08) were the most prominent regions identified in the evaluation model (Fig. 2b upper left & 2c), thus being highly sensitive for tracking the entire dimension from punishment to reward. These areas coincide with the terminal regions of the dopamine neuron projections from the ventral tegmental area (VTA), i.e. the meso-corticolimbic dopamine system [20-22]. For the readiness model, however, the signals were more widely dispersed across cortical and subcortical areas, including motor-somatosensory, salience and attention networks, and regions such as the dorsal striatum (DS, Peak MNI: [8, 10, 4], $t_{1,927}$ = 32.80, Cohen's D = 0.75) and thalamus (THA, Peak MNI: [13, -6, 16], $t_{1,927}$ = 24.66, Cohen's D = 0.56, Cluster: 2267 voxels, $p_{\text{FWE-corr}}$ = 1.11E-16) (Fig. 2b upper right & 2c), consistent with their engagement in processing both reward and punishment [23].

Respective neural circuits

We then investigated whether the neural representations of evaluation and readiness processes were underpinned by putative neural circuits, in particular those modulated by the midbrain dopaminergic projections originating from either the substantia nigra pars compacta (SNc) or the VTA, which plays a central role in reward prediction and approach [20, 21]. We found regions of the evaluation model with higher functional connectivity (FC) to VTA than to SNc (*paired t*-test: t_{183} = 14.84, Cohen's D = 1.10, p < 10E-32, Fig. 3a), and regions of the readiness model with higher FC to the SNc than to the VTA (*paired t*-test: t_{183} = 3.63, Cohen's D = 0.27, p = 0.0004, Fig. 3a) based on 7T high-resolution resting-state fMRI data from the Human Connectome Project [24]. Further, we extracted the *t*-maps of the difference between the seed-based FC from VTA and SNc (Extended Data Fig. S2a-c), which was exhibited high similarities, although in opposite directions, with the *t*-maps of both evaluation (r = 0.22, p_{adj} < 10E-20) and readiness (r = -0.12, p_{adj} < 10E-12, Fig. 3b) models. Thus, the separate VTA and SNc dopamine projections could be the underlying source of

evaluation and readiness processes, respectively.

Independence of evaluation and readiness

We further demonstrated that the above spatially overlapping cognitive processes modulated by distinct neural pathways were indeed functionally independent, which could be directly inferred from uncorrelated signal components at the co-activated regions (see Methods for the detailed proof). Based on our simulation results, only if the compound signals were indeed a combination of independent signals, the decomposed signals could be uncorrelated ($|r_{mean}| < 0.001$, the 'Independent' model). Otherwise, the decomposed signals were highly correlated and hence inseparable as modulations of latent signals (the 'One Signal' model: $r_{mean} = 0.54$; the 'Push and Pull' model: $r_{mean} = -0.45$; Extended Data Fig. 1B & Extended Data Table 2).

In this study, we found that the signals attributed to evaluation and N-shape models (dependent signals: $r_{mean} = -0.093$, 95% CIs = [-0.114 to -0.073], $p_{bootstrap} < 0.0001$ based on 10000 bootstrap) together described the sensitivity of evaluation from punishment to reward. Further, signals of evaluation and N-shape models were independent (evaluation *vs* readiness: $r_{mean} = 0.006$, 95%CIs = [-0.009, 0.021], $p_{bootstrap} = 0.4142$, 99.5% voxels with $r \in [-0.1,0.1]$, i.e. less than a meaningful small effect size; evaluation *vs* W-shape: $r_{mean} = -0.008$, 95% CIs = [-0.025, 0.009], $p_{bootstrap} = 0.3358$, 99.3% voxels with $r \in [-0.1,0.1]$; N-shape *vs* readiness: $r_{mean} = -0.001$, 95% CIs = [-0.015, 0.012], $p_{bootstrap} = 0.8432$, 99.3% voxels with $r \in [-0.1,0.1]$) of those attributed to the readiness and W-shape models (dependent signals: $r_{mean} = -0.159$, $p_{bootstrap} < 0.0001$), which together described the differentiated engagement of readiness from the neutral condition to reward/punishment conditions (Fig. 4a). Hence, the observed unbalanced sensitivity towards reward and punishment, such as VS and vmPFC, could be parsed into two spatially overlapped though functionally independent signal components, i.e. a point-symmetric evaluation process and a line-symmetric readiness process (Fig. 4c).

Complementary components from DeCoP

Additionally, the complementary N-shape and W-shape models account for the

deviation from the latent evaluation and readiness signals of the proposed evaluation and readiness models respectively. Complementary to the evaluation model, the N-shape model was only observed with significant signals in the primary visual cortex (BA 17; Peak MNI: [4, -81, 1], $t_{1,927}$ = 7.65, Cohen's D = 0.17, Cluster: 233 voxels, $p_{\text{FWE-corr}}$ = 2.91E-05, Fig. 2b lower left & 2c). For the W-shape model, as being complementary to the readiness model, the most prominent regions were bilateral anterior insula (aINS, BA 38, Peak MNI: [49, 25, -9], $t_{1,927}$ = 14.83, Cohen's D = 0.34; Cluster: 1177 voxels, $p_{\text{FWE-corr}}$ = 4.41E-05) and anterior cingulate cortex (ACC, BA 32, Peak MNI: [7, 49, 22], $t_{1,927}$ = 11.51, Cohen's D = 0.26; Cluster: 881 voxels, $p_{\text{FWE-corr}}$ = 2.87E-10, Fig. 2b lower right & 2c). Therefore, the signal strength of the additional complementary orthogonal contrasts could provide a useful measurement of the distance between the latent independent signals and the proposed models (see Methods for more details). Converging evidence indicated that most brain regions distinguish reward from punishment signals with their relative rank. In other words, the brain simplifies the scales of the different values when processing reward/punishment information, hence processing highly abstract information only. However, the bilateral anterior insula (aINS) and dorsal anterior cingulate cortex (dACC), commonly referred to as the salience network, were most likely tracking the parametric nature of the experimental design (i.e. [-5, -0.2, 0, 0.2, 5]; Extended Data Fig. 3-4 & Extended Data Table 3; also see Supplementary Information for more details). These results were consistent with the role of aINS and dACC in updating and maintaining subjective value information [25, 26].

Differential impacts on task performance

We further implemented a weighted voxel co-activation network analysis (WVCNA) to capture the most informative brain-wide signal clusters [27] and identified 55 and 194 clusters for the evaluation and readiness processes, respectively. These clusters could be further divided into four and five subnetworks by hierarchical clustering, respectively (see Supplementary Information for more details, Extended Data Fig. 5 & Extended Data Table 4). Again, we observed brain-wide low correlations

between evaluation and readiness clusters (r_{mean} = 0.01, $p_{bootstrap}$ = 0.1621; Fig. 3B), hence further supporting their neural functional independence.

We then investigated the effects of decomposed signals on task performance using the canonical correlation analysis (CCA) [28, 29], and found associations between variations in the neural signal and task performance across three condition categories (i.e. reward, neutral and punishment) for both evaluation and readiness: reaction time (evaluation: adjusted η^2 ($adj\text{-}\eta^2$) = 0.020, $p_{perm} < 0.001$; readiness: $adj\text{-}\eta^2$ = 0.075, $p_{perm} < 0.001$) and accuracy (evaluation: $adj\text{-}\eta^2$ = 0.025, $p_{perm} < 0.001$; readiness: $adj\text{-}\eta^2$ = 0.079, $p_{perm} < 0.001$; Extended Data Table 5-6).

Next, based on identified behavioural components from the CCA results, we investigated how task performance received differential contributions from decomposed latent evaluation and readiness signals, especially in spatially overlapping regions, for instance the vmPFC, dACC, and bilateral striatum. For the evaluation signals, both faster reaction times and higher accuracy demonstrated similar first behavioural components, i.e. loading heavily on both reward and punishment conditions but not on the neutral condition. Both components were associated with reduced sensitivity of evaluation processing in the left VS, vmPFC and dACC (Fig. 5a-b & Extended Data Table 5-6), thus highlighting that the evaluation process is engaged similarly for either the reward or punishment signal, which also helps to explain the lack of difference in task performance beween reward and punishment trials. On the contrary, suppressed readiness processing in left VS and dACC was uniformly associated with faster reaction times across all three experiment conditions. We also observed a competing readiness process featuring with a greater engagement of a task-preparatory and motor-response network (i.e. the supplementary motor area SMA and somatosensory-motor cortices) that could led to faster reaction times across all three experiment conditions (represented as the first behavioural component, Fig. 5d right & Extended Data Table 5). In terms of accuracy, however, readiness signals in the right aINS and dACC (i.e. the salience network) produced opposite effects in the presence or absence of valence signals: in reward/punishment trials (i.e. the first behavioural component), higher accuracy was associated with reduced sensitivity (Fig. 5d left),

whereas in neutral trials (i.e. the second behavioural component), the relationship was reversed, with higher accuracy associated with more readiness (Fig. 5d right & Extended Data Table 6).

In conclusion, we demonstrated that neural processing for evaluation and readiness contribute differentially to task performance. The lack of cognitive associations between task performance and signal values (see Fig 1c) was because neural processing for both evaluation and readiness contributed equivalently to task peformance in reward and punishment conditions.

Theoretical neuronal encoding models

Above, we have demonstrated the existence of two spatially overlapping, though functionally independent neural representations in the brain encoding value and salience information, thus indicating two distinct patterns of neuronal response at the cellular level. However, it remains unclear how neuronal populations can encode two distinct aspects of information from the same input. Here, we established an integrated three-layer spike neural network that could translate the same input into value and salience outputs, respectively (Fig. 6).

Remarkably, while the models for value and salience outputs were trained individually, both models demonstrate a surprisingly high convergence on the input and hidden layers. Specifically, in both models, neurons in the input layer all had a linear response to the value of signals (i.e. from lower to higher activations according to the signal strength from punishment to reward), and neurons in the hidden layer were formed in two groups: one was activated by punishment inputs ("punishment neurons") , the other being activated by reward inputs ("reward neurons") (Fig. 6). The co-existence of reward and punishment neurons has been supported by findings across multiple species [30-34]. Further, the connections between the input and hidden layers in both models were also highly similar (value model: μ_{weight} = 0.0187, excitatory/inhibitory ratio (E/I ratio) = 1.8825, μ_{bias} = 3.7294; salience model: μ_{weight} = 0.0184, E/I ratio = 1.8409, μ_{bias} = 3.7489; Extended Data Fig. 6), thus indicating that the input and hidden layers of both neural networks were highly robust and

homogeneous, and could be represented by the same group of neurons.

Both neural networks mainly differ in the output layers. For the value model, neurons in the output layer were inhibited if connecting to the 'punishment neurons' in the hidden layer and activated if connecting to the 'reward neurons', hence demonstrating linear output from punishment to reward (Fig. 6 & Extended Data Fig. 6). For the readiness model, however, there are two groups of neurons in the output layer: one group is activated when connecting to the "punishment neurons" but inhibited if connecting to the "reward neurons" from the hidden layer. In contrast, the other group was reversely inhibited when connecting to the "reward neurons" but activated if connecting to the "punishment neurons". Hence, the net outputs for reward and punishment stimuli were equivalent (Fig. 6 & Extended Data Fig. 6).

Altogether, this integrated three-layer neural network could encode the same input into distinct value and salience outcomes, thus providing a plausible population neuronal model underlying the spatially overlapping, though functionally independent neural representations of evaluation and readiness, which may provide further insight into the real-world neuronal encoding system.

Discussion

In the present study, we have successfully disentangled two functionally independent (i.e. evaluation and readiness) processes from complex neurobehavioural signals during reward/punishment processing by the novel approach. Our findings provide insight into commonly ambiguous observations in fMRI tasks which involve multiple interferential latent behavioural or cognitive processes. For example, vmPFC, as a key node in the neural circuitry underlying reward processing and value-based decision making [35-37], was paradoxically 'inactive' during the reward vs neutral contrast. This unexpected 'inactivation' can now be understood as a product of a trade-off between two independent processes: activation by reward stimuli (i.e. of the evaluation process) and deactivation as part of the default mode network (i.e. of the readiness process). Furthermore, our findings also demonstrated that the independence of evaluation and readiness processing in the brain, putatively is mediated by differential

neural circuits including the VTA and SNc respectively. This finding provides novel evidence that the reward processing is linked to the midbrain dopaminergic system and that evaluation and readiness processes involve distinct underlying neural mechanisms [7, 22, 38]. Motivated by these findings, we formulated an integrated theoretical neuronal population-coding model to illustrate a plausible neuronal mechanism underlying the segregation of value and salience signals from the same input. The two discrete neuronal populations revealed in the hidden layer, which respectively responds to reward and punishment signals, were also supported by previous studies of dopamine neurons in rodent and primates, especially in the VTA and the VS [30-34]. We thus proposed a unified dopaminergic signal processing system that could bridge the gap between the neuronal signal encoding (at the cellular level) and the neural representation of encoded signals (at the metabolic or functional level), which may significantly advance our understanding of the neural basis of reward/punishment processing.

Further, our novel approach also enables direct statistical inference concerning the functional independence among decomposed latent neurobehavioural processes based on predefined orthogonal latent contrasts. This demonstration may have radical implications for analysing experimental designs of theoretical neurobehavioural models. While existing research frameworks have hitherto attempted to identify spatially separated brain regions that activate specifically under a particular neurobehavioural model [5, 18], such a 'specific' activation is highly subjective to the selected threshold for significance and hence may not be truly 'specific'. More problematically, even if an activation is indeed specific to a particular model and null in the other, their underlying signals might still be related. For instance, while the N-shape model in the present study was barely activated brain-wide, it nevertheless showed strong negative correlations with the evaluation model in voxels that were 'specifically' activated for the evaluation models, and hence both signals were not independent of one another. Therefore, the statistical framework provided by our novel approach is vital for any meaningful inference of decomposed independent signals. Moreover, such a statistical framework enables a computational decomposition for any potentially independent

neurobehavioural processes, as long as the experimental design allows a meaningful orthogonal decomposition. We therefore expect this new approach to promote new study designs for cognitive processes that are theoretically distinct but almost inseparable through common experimental designs.

Finally, our analytical framework could comprehensively describe any possible outcomes across all experimental conditions. Complementary to the proposed theoretical neurobehavioural models, the other orthogonal components specified from the same theoretical framework could also provide valuable information. For instance, in the present study, the complementary N-shape and W-shape models, were highly correlated with the evaluation and readiness components, respectively. Therefore, both components modified the response to small monetary stimuli of the corresponding primary models during reward/punishment anticipation. This led to the finding that dACC encoded the exact monetary magnitude of the experimental design in both evaluation and readiness models, whereas most other regions encode only highly abstracted information. This observation is consistent with the role of dACC in updating and maintaining subjective value information [25, 26]. Besides dACC, an unexpected increase in the neutral condition was observed for bilateral aINS, rendering the best model in fitness as the W-shape model, instead of the V-shape readiness model. In fact, the W-shape activation has also been observed in several previous studies on reward-related decision making [3, 17], though without further discussion. The aINS was seemingly involved in two situational processes in regulating task performance, in that higher engagement of aINS could lead to better performance in the absence of reward or punishment signals, but it is the suppressed aINS that was associated with better performance in the reward/punishment trials. This observation may help to understand the W-shape activation of aINS as a combination of two situational processes (for instance, positive and negative V-shape activations). Hence, DeCoP could further strengthen our understanding of latent neurobehavioural processes through additionally retrieving complementary, though not necessarily independent, components.

In summary, we have developed and evaluated a novel signal decomposition strategy, 'DeCoP', to dissociate behavioural processes that confound the observation of

functional neuroimaging signals. Through DeCoP we demonstrated the functional independence of evaluation and readiness processing in the brain, putatively modulated differentially by neural circuits targeting VTA and SNc. We also proposed an integrated theoretical neuronal population-coding model to illustrate a plausible neuronal mechanism underlying the segregation of evaluation and readiness by distinct midbrain dopaminergic projection systems. We also found that most brain regions encoded signals based on abstract information instead of the observed exact monetary magnitude scale, except for the salience network, i.e. dACC and aINS. We expect that DeCoP can be applied usefully to elucidate many other comparably ambiguous data-sets and enhance experimental designs for complex cognitive processing.

Methods

Participants

The dataset used for this study was selected from Annual Curated Data Release 2.01 (https://data-archive.nimh.nih.gov/abcd) of the Adolescent Brain Cognitive Development (ABCD) cohort, which recruited 11,875 children between 9–11 years of age from 21 sites across the United States [19]. The study conforms to each site's Institutional Review Board's rules and procedures, and all participants provide informed consent (parents) or informed assent (children). More details of the subjects and the data collection are provided at the ABCD website (https://abcdstudy.org/scientists/protocols/) and are also described previously [19].

Magnetic resonance imaging (MRI) data in the ABCD study were collected from different 3T scanner platforms (i.e. Siemens Prisma, General Electric MR750 and Philips Achieva dStream). To minimise biases introduced by multiple platforms, we only included MRI data from the most frequent manufacturer Siemens Prisma, i.e. 5968 participants from 13 sites. By examining the similarity of brain activations across these 13 sites, we selected 2326 participants from 4 sites with consistent activation patterns. Furthermore, the data with poor registration (by visual check) and high head motion (mean framework displacement (FD) > 0.5 mm) were excluded. Hence, 1939 quality-controlled participants were included in the following analysis and the demographic characteristics of these participants are summarised in Extended Data Table 1. In the further analyses, the age, gender, handedness, race, site informance and mean FD of participants were included as the covariates.

Monetary incentive delay (MID) task design

A modified version of the MID task was used to examine brain activation during monetary reward anticipation and receipt [39], which consists of five levels of incentive: large loss, small loss, neutral, small win and large win (i.e., -5.0 $, -0.2 $, 0 $, 0.2 $ and 5.0 $ respectively). In each trial, participants were first presented with one of three cue shapes (circle, square or triangle) that indicated the trial condition (of win, loss, or neutral, respectively), as well as the amount of money involved. This cue presentation

(2,000 ms) was followed by a jittered anticipatory delay (1,500-4,000 ms) of fixation on a black crosshair. Subsequently, a blank target cue (with the same shape as the previously presented cue) emerged and required the participants to press a response button before the target disappeared to win or avoid loss. With a tracking algorithm, the time of the target on the screen was dynamically manipulated (i.e., 150 ms-500 ms) to maintain a 60% success rate for each participant. After a short delay, feedback of the current trial (i.e., the amount of monetary gain or loss) and the accumulated reward so far were presented for 1,500-1,850 ms (Fig. 1a). During the anticipation phase, participants underwent 50 trials in total (i.e., 10 trials per incentive degree). Participants had first completed a practice session outside the scanner before completing two sessions of the MID task with fMRI recording (approximately 5.5 minutes each).

We first compared the task behaviour outcomes (i.e., the reaction time (RT) and accuracy) between the salient (i.e., reward or punishment) and neutral contions acorss the participants by paried *t-test*. We next set a general linear model to estimate the effects of the putative contrasts (i.e., value model: [-2 -1 0 1 2] and salience model: [2 1 0 1 2]) on the task behaviour outcomes at the individual level. Then the group-level effects were obtained by one sample *t-test*.

Image acquisition and preprocessing

Imaging protocols were harmonised across sites and scanners. 3-dimensional T1-weighted images (1.0 mm isotropic, TR = 2500 ms, TE = 2.88 ms) were acquired with a gradient-echo sequence for anatomical localisation and high spatial (2.4 mm isotropic) and temporal (TR = 800 ms) resolution MID-task-based fMRI was acquired with echo-planar imaging (EPI) sequence. The detailed MRI acquisition protocol is described elsewhere [19]. All functional images were preprocessed with the same preprocessing procedure by suggested protocols from FMRIB's Software Library (FSL v5.0.9), Advanced Normalization Tools (ANTs v1.9.2) and Analysis of Functional NeuroImages (AFNI v18.3.03). Concretely, the whole preprocessing procedure included the following steps: (i) brain extraction (ANTs antsBrainExtraction), nonlinear registration to MNI space (ANTs antsRegistrationSyN) for structural images; (ii) rigid

realignment to adjust for motion (FSL MCFLIRT) and field map correction (FSL TOPUP) for functional images; (iii) co-registration to a high-resolution T1 image and normalisation to 3 mm isotropic MNI standard space (ANTs antsRegistrationSyN) and (iv) spatial smoothing with a 6mm full-width at half-maximum (FWHM) Gaussian kernel (AFNI 3dBlurToFWHM) and detrending (AFNI 3dDetrend).

First-level analysis of task-based fMRI

At the first-level analysis, we set up a general linear model to estimate the effects of the task conditions at the individual level with SPM, which contained 20 task condition regressors (i.e. Target (Hit or Miss) * Phases (Anticipation, Feedback) * Task Conditions (Large-Loss, Small-Loss, Neutral, Small-Win or Large-Win)) and additional covariate regressors (i.e., 24 motion-related parameters: 6 rigid-body motion parameters, their first temporal derivatives and 12 corresponding squared items; and mean signals of both white matter and ventricles). All regressors were convolved with a double-gamma HRF, and no orthogonalisation of regressors was applied. For BOLD signals, drift was modelled with the DCT basis, and a cut-off of 128 s was applied (SPM defaults). Finally, the autocorrelation was modelled as a global approximate AR(1) in SPM.

Orthogonally Decoding multi-Cognitive Processes

In the present study, we propose a novel approach to decompose each participant's brain activations at varied conditions (denoted as y) with a set of orthogonal basis $\mathbf{x} = (x_i, \ldots x_k)$, where each vector could represent a predefined signal model, e.g. evaluation or readiness. Specifically, 'orthogonal' here means that any pairwise covariances of vectors all equal zero, i.e. $Cov(x_i, x_j) = E(x_i, x_j) - E(x_i)E(x_j) = 0$. In this way, the regression coefficients $\boldsymbol{\beta} = (\beta_1, \ldots \beta_k)$ (i.e. the strength of signals for each individual) estimated from a multiple linear model with all vectors were the same as those estimated univariately (of simple linear models), i.e.

$T(\beta_i \mid y, \mathbf{x}, \boldsymbol{\beta}_{-i}) = T(\beta_i \mid y, x_i)$, where $T(\cdot)$ stands for the best linear unbiased estimator.

We propose that the above individual level orthogonal decomposition eliminates spurious correlations of signal components (i.e. β) introduced by related vectors (i.e. x_i are correlated), thus allowing us to make meaningful inferences regarding signal independence at the population level. Here, we only describe a simple proof for the purpose of illustration, where only two orthogonal vectors were involved. Let y_i denote the vector of activations across all conditions of the ith individual, and x_{1i} and x_{2i} denote the two predefined independent orthogonal models of input signals, where $Cov(x_{1i}, x_{2i}) = 0$, and β_{1i} and β_{2i} denote the corresponding regression coefficients, i.e. the signal strengths. We could then have the following linear model:

$$y_i = \beta_{1i} x_{1i} + \beta_{2i} x_{2i} + \varepsilon .$$

We first show that orthogonal settings of x_{1i} and x_{2i} are necessary for a meaningful independent decomposition of signals. The covariance and variance conditioned on x_{2i} could be easily derived as:

$$Cov\left(x_{1i}, y_i \mid x_{2i}\right) = Cov\left(x_{1i}, y_i\right) - Cov\left(x_{1i}, x_{2i}\right) \cdot Cov\left(y_i, x_{2i}\right) \Big/ Var\left(x_{2i}\right)$$

and

$$Var\left(x_{1i} \mid x_{2i}\right) = Var\left(x_{1i}\right) - Cov\left(x_{1i}, x_{2i}\right)^2 \Big/ Var\left(x_{2i}\right) .$$

Similar results can also be acquired for the covariance/variance conditioned on x_{2i}. Therefore, we establish the following relationship between the least square estimations (LSEs) of β_{1i} and β_{2i}:

$$
\begin{aligned}
&\frac{Cov(x_{1i}, y_i)}{Var(x_{1i})} - \beta_{1i} \\
&= \frac{Cov(x_{1i}, y_i)}{Var(x_{1i})} - \frac{Cov(x_{1i}, y_i \mid x_{2i})}{Var(x_{1i} \mid x_{2i})} \\
&= \frac{Cov(x_{1i}, y_i)}{Var(x_{1i})} - \frac{Cov(x_{1i}, y_i) - \frac{Cov(x_{1i}, x_{2i}) \cdot Cov(x_{2i}, y_i)}{Var(x_{2i})}}{Var(x_{1i}) - \frac{Cov(x_{1i}, x_{2i})^2}{Var(x_{2i})}} \\
&= \frac{Cov(x_{1i}, x_{2i}) \cdot Cov(x_{2i}, y_i) \cdot Var(x_{1i}) - Cov(x_{1i}, y_i) \cdot Cov(x_{1i}, x_{2i})^2}{Var(x_{1i})^2 \cdot Var(x_{2i}) - Var(x_{1i}) \cdot Cov(x_{1i}, x_{2i})^2} \\
&= \frac{Cov(x_{1i}, x_{2i})}{Var(x_{1i})} \cdot \frac{Cov(x_{2i}, y_i) - \frac{Cov(x_{1i}, x_{2i}) \cdot Cov(x_{1i}, y_i)}{Var(x_{1i})}}{Var(x_{2i}) - \frac{Cov(x_{1i}, x_{2i})^2}{Var(x_{1i})}} \\
&= \frac{Cov(x_{1i}, x_{2i})}{Var(x_{1i})} \cdot \frac{Cov(x_{2i}, y_i \mid x_{1i})}{Var(x_{2i} \mid x_{1i})} \\
&= \frac{Cov(x_{1i}, x_{2i})}{Var(x_{1i})} \cdot \beta_{2i}
\end{aligned}
$$

.

Clearly, unless $Cov(x_{1i}, x_{2i}) = 0$, β_{1i} could always be expressed as a function of β_{2i}, and hence can never be independent of each other. The above derivations, therefore, prove the necessity of using orthogonal vectors for meaningful signal decomposition.

Meanwhile, by setting $Cov(x_{1i}, x_{2i}) = 0$, and realising that the LSE of β_{1i} in the absence of x_{2i} from the regression model (1) (i.e. reduced to a simple linear model) is $\beta'_{1i} = Cov(x_{1i}, y_i)/Var(x_{1i})$, we could immediately have $\beta'_{1i} = \beta_{1i}$. Thus with orthogonal x_{1i} and x_{2i}, estimations from a multiple linear model will be the same as those univariately estimated from simple linear models.

We then show that the population-level correlation analyses of β_{1i} and β_{2i} derived above provide meaningful statistical inferences of signal independence. For simplicity, assume that we could rewrite β_{2i}, the signal strength of model x_{2i}, into a sum of two independent components, i.e. $\beta_{2i} = \beta'_{2i} + \gamma_i \beta_{1i}$ where β'_{2i} is independent of β_{1i}, i.e. $Cov(\beta'_2, \beta_1) = 0$, and the parameter γ_i denotes the proportion of overlapped signals

with model x_{1i}, and is independent of β_{1i}, i.e. $Cov(\gamma, \beta_1) = 0$. We could then calculate the population-level correlation of β_{1i} and β_{2i} as:

$$\begin{aligned} Cov(\beta_1, \beta_2) &= Cov(\beta_1, \beta_2' + \gamma\beta_1) \\ &= Cov(\beta_1, \beta_2') + Cov(\beta_1, \gamma\beta_1) \\ &= E(\gamma\beta_1^2) - E(\beta_1)E(\gamma\beta_1) \\ &= E(\gamma\beta_1^2) - E(\gamma)E(\beta_1^2) + \left(E(\gamma)E(\beta_1^2) - E(\beta_1)E(\gamma)E(\beta_1)\right) \\ &= Cov(\gamma, \beta_1^2) + E(\gamma)Var(\beta_1) \\ &= E(\gamma)Var(\beta_1) \end{aligned} \quad ,$$

which only equals 0 if either $E(\gamma) = 0$, i.e. the population mean signals of both models are not a function of each other, or $Var(\beta_1) = 0$, i.e. one of the signals is invariant across the population, and hence again is not dependent on the other signal. Either way, the signals of both models are indeed independent, and hence we could have $Cov(\beta_1, \beta_2) = 0 \Leftrightarrow \beta_1 \perp\!\!\!\perp \beta_2$. In conclusion, this two-stage approach can be used for statistical inference concerning the dependence of decomposed signals.

To illustrate the above theoretical derivations, we conducted simulation analyses to evaluate the performance of DeCoP on three different complex signal models, namely the "independent-signal model", where each observed signal consists of two independent inputs ($\beta_{1i} \perp\!\!\!\perp \beta_{2i}$, and hence $Cov(\beta_1, \beta_2) = 0$), and two dependent-signal models, i.e. the 'single signal model' with $\beta_{2i} = \gamma_i\beta_{1i}$ (assume $E(\gamma) > 0$, and hence $Cov(\beta_1, \beta_2) > 0$), and the 'push-and-pull model' with $\beta_{2i} + \gamma_i\beta_{1i} = c_i$ (assume $E(\gamma) > 0$, and hence $Cov(\beta_1, \beta_2) < 0$). For simplicity, the signal overlapping parameter γ_i was set as a constant (i.e. 0 for the independent-signal model and 1 in both dependent-signal models); the observed signals (y_i in equation 1) were simulated from [-2, -1, 0, 1, 2] to [2, 1, 0, 1, 2] with an increment of [0.2, 0.1, 0, 0, 0] at each step, i.e. [-2, -1, 0, 1, 2], [-1.8, -0.9, 0, 1, 2], …, [1.8, 0.9, 0, 1, 2], [2, 1, 0, 1, 2]; and the orthogonal vectors were fixed as x_{1i} = [2, 1, 0, 1, 2] and x_{2i} = [-2, -1, 0, 1, 2]. Therefore, for the 'single signal model', y_i was directly set as the observed signals plus a random noise $N(0,1)$. For the 'push-and-pull model', at the ith simulation step,

by setting $c_i = 0.05\times(i-1)+N(0,1)$, $\beta_{1i} = c_i + N(0,1)$ and $\beta_{2i} = 1-c_i+N(0,1)$, we could then simulate $y_i = \beta_{1i}x_{1i} + \beta_{2i}x_{2i}$. Clearly, at the population-level, we have $Cov(\beta_1,\beta_2) = E_i^2(c) - E_i(c^2) = -Var(c) \neq 0$, and hence β_1 and β_2 are dependent. For the 'independent-signal model', at the *i*th simulation, by setting $c = 0.05\times(i-1)$, $\beta_{1i} = c + N(0,1)$ and $\beta_{2i} = 1-c+N(0,1)$, we could also simulate $y_i = \beta_{1i}x_{1i} + \beta_{2i}x_{2i}$, where, however, one would expect $Cov(\beta_1,\beta_2) = 0$. It is notable that while the simulation models of 'push-and-pull' and 'independent-signal' are rather similar, they are fundamentally different. The reason lies in the fact that the constant c in the 'independent-signal model' is invariant across individuals and solely determined by the predefined form of observed signals, and hence the signal strengths β_{1i} and β_{2i} do not dependent on each other. However, in the 'push-and-pull model', the form of observed signals only determined the expectation $E_i(c)$, and hence both β_{1i} and β_{2i} are nevertheless the functions of c_i that varies across individuals, and thus are not independent. For each model, we simulated with 1000 independent individuals for 1000 times, and the detailed results of simulations are shown in Extended Data Fig. 1b and Extended Data Table 2.

Functional connectivity (FC) based on resting-state fMRI data

A total of 184 participants' preprocessed high-resolution (7T) resting-state fMRI data were collected from the Human Connectome Project (HCP) dataset [24]. Total FC (Z-score of Pearson Correlation) from evaluation and readiness activation activations regions to the voxels in the brainstem (Fig. 3a left), which were masked with AAL3 atlas [40] and from VTA and SNc to the whole brain were examined respectively. A paired *t-test* was used to estimate which brain region had a stronger FC with the activation region. The similarity between patterns of activation and FC was represented by Pearson's correlation coefficient *r*. Due to the high correlations among voxels, the degree of freedom was adjusted to the number of components that accumulatively

explain over 95% variance of brain activations based on the principal component analysis.

Measurement of modifying effects

As N-shape and W-shape models can be considered modifiers of evaluation and readiness models, respectively, their strength (i.e. the activation level) can be used to measure the deviance from the proposed model settings, i.e. the exact scale or the relative scale. Thus we computed the standardised mean $((t_{relative} + t_{exact})/\max(abs(t_{relative}), abs(t_{exact})))$ to evaluate the prevailing settings, where $t_{relative}$ represents the t-statistics of the activation for N-shape or W-shape models under the relative-scale setting, and t_{exact} represents the t-statistics of the activation for N-shape or W-shape models under the relative-scale setting. When the observed signal falls somewhere between the relative-scale and exact-scale settings, it is readily observable that $t_{relative}$ would be positive and t_{exact} would be negative. Therefore, $abs(t_{relative}) > abs(t_{exact})$ would prefer the exact-scale setting, and the standardised mean ranges from 0 to 1, whereas $abs(t_{relative}) < abs(t_{exact})$ would prefer the relative-scale setting, and the standardised mean ranges from -1 to 0. It is notable that meaningful settings other than this may also be possible. For instance, the response of the small stimuli could be identical to the large stimuli in the observed signal, thus $t_{exact} < t_{relative} < 0$, and the standardised mean could be well smaller than -1. We further performed *F-test* on the strength of the decomposed components in the brain regions which favour the different scale settings and compared the coincidence degree for the task performance.

Weighted voxel coactivation network analysis (WVCNA)

The R package WGCNA [41] was implemented to conduct the WVCNA [27], which identifies activation clusters of both evaluation and readiness models across the brain. The final dataset used for WVCNA included 1,912 participants with 3365 voxels for the evaluation model and 1900 participants with 10932 voxels for the readiness model after removing null data and outliers. We transferred most parameters as default settings from previous studies [42], except for the soft-threshold parameters, which were set to

seven based on the scale-free topology criteria, incidentally identical to those estimated for the MID task from a different cohort [42]. The stabilities of the generated modules were assessed through bootstrapping. The hierarchical clustering was then applied on the distance matrices among the identified activation modules and, together with the cut-tree function, these modules were further clustered into subnetworks with a static cut at the half of the maximum cluster height (i.e. 1.5 for the evaluation and 2.3 for the readiness).

Canonical correlation analysis (CCA)

CCA has been widely used to investigate the overall correlation between two sets of standardised variables [28]. Due to high intra-correlations in both brain networks and task performances, multicollinearity was a potential risk factor jeopardising the validity of the subsequent statistical inference. Therefore, we adopted the ridge-restricted CCA proposed in a previous reference, where the regularised parameter was set as 0.1 [42]. For each correlation, the P-value or significance level was determined using the permutation test, where the individual IDs of task performances were randomly shuffled at each iteration to generate the null distribution of the corresponding test statistics.

Further, we used the adjusted eta square (η^2) to represent the proportion of mutually explained variance between the two sets of variables, as well as controlling for the inflation in η^2 caused by overfitting:

$$\eta^2_{adj} = 1 - \frac{1-\eta^2}{1-\eta^2_0}$$

where η^2_0 represents the expected η^2 under the null hypothesis that there is no relationship between the two sets of variables (that is, it acts as a measure of inflation in $\eta 2$), and can be directly estimated through the permutation test.

Simulation of neuronal population-coding models by artificial neural networks (ANN)

We trained a three-layer ANN with full connected fashion which contains 24 neurons in each layer and we used Relu function as activate function. For evaluation

model networks, we expected the model can map the input [-20, 20] into [0, 4]. For readiness model networks, we split the output response into two parts, each part response to positive and negative input respectively. To obtain the identical mean output as evaluation model, the readiness model mapped [-20, 0], [0, 20] into [2, 0], [0, 2]. We designed a training task sequence from easy to hard (curriculum learning) in training. For example, we first set 5 points the model need to learn, then 10 points, 100 points and etc. To constrain the distribution of presynaptic weight of each output neuron, we set a regularization term base on the variance of weight matrix of the last layer for training. When visualization, we sorted the position of neurons in hidden layer and output layer base on the sum of their presynaptic weight.

Data availability

ABCD data are available from a dedicated database: https://abcdstudy.org. Human Connectome Projects data are available from: https://www.humanconnectome.org.

Code availability

Custom code that supports the findings of this study is available from the corresponding author upon request. All data needed to evaluate the conclusions in the paper are present in the paper and/or the Supplementary Information. Additional data related to this paper may be requested from the authors.

Acknowledgments

This work received support from the following sources: National Key Research and Development Program of China (No. 2019YFA0709502 and No. 2018YFC1312900), the National Natural Science Foundation of China (No. 91630314 and No 81801773), the 111 Project (B18015), the Key Project of Shanghai Science &Technology Innovation Plan(16JC1420402), Shanghai Municipal Science and Technology Major Project (2018SHZDZX01) and Zhangjiang Lab and the Shanghai Pujiang Project (No. 18PJ1400900). The funders had no role in study design, data collection and analysis, decision to publish or preparation of the manuscript.

Author Contributions:

Conception or Design of the Study: C.X., T.J., T.W.R. and J.F.. Manuscript Writing and Editing: S.X. and T.J. wrote the manuscript; T.W.R. and J.F. edited the first draft; all authors critically reviewed the manuscript. Imaging Data Preprocessing: S.X., C.X. and W.C.. Visualization: S.X., C.X. and T.J.. Data Analysis: S.X., C.X., Z.Z., J.K. and G.S. conducted all the statistical analyses, under the instruction of T.J. and J.F.. Results Interpretation: T.J., T.W.R. and J.F.. Supervision of the Study: T.J. and J.F.. Funding Acquisition: T.J. and J.F..

Competing Interests:

The authors declare no competing interests.

Reference

1. Price, C.J. & Friston, K.J. Functional ontologies for cognition: The systematic definition of structure and function. *Cogn Neuropsychol* **22**, 262-275 (2005).
2. Kahnt, T., Park, S.Q., Haynes, J.D. & Tobler, P.N. Disentangling neural representations of value and salience in the human brain. *Proc Natl Acad Sci U S A* **111**, 5000-5005 (2014).
3. Zhang, Z.*, et al.* Distributed neural representation of saliency controlled value and category during anticipation of rewards and punishments. *Nat Commun* **8**, 1907 (2017).
4. Friston, K.J. Modalities, modes, and models in functional neuroimaging. *Science* **326**, 399-403 (2009).
5. Kragel, P.A., Koban, L., Barrett, L.F. & Wager, T.D. Representation, Pattern Information, and Brain Signatures: From Neurons to Neuroimaging. *Neuron* **99**, 257-273 (2018).
6. Fellows, L.K. The cognitive neuroscience of human decision making: a review and conceptual framework. *Behav Cogn Neurosci Rev* **3**, 159-172 (2004).
7. Zald, D.H. & Treadway, M.T. Reward Processing, Neuroeconomics, and Psychopathology. *Annual Review of Clinical Psychology* **13**, 471-495 (2017).
8. Juechems, K.*, et al.* A Network for Computing Value Equilibrium in the Human Medial Prefrontal Cortex. *Neuron* **101**, 977-987 e973 (2019).
9. Kennerley, S.W., Behrens, T.E. & Wallis, J.D. Double dissociation of value computations in orbitofrontal and anterior cingulate neurons. *Nat Neurosci* **14**, 1581-1589 (2011).
10. Lebreton, M., Jorge, S., Michel, V., Thirion, B. & Pessiglione, M. An automatic valuation system in the human brain: evidence from functional neuroimaging. *Neuron* **64**, 431-439 (2009).
11. Strait, C.E., Blanchard, T.C. & Hayden, B.Y. Reward value comparison via mutual inhibition in ventromedial prefrontal cortex. *Neuron* **82**, 1357-1366 (2014).
12. Tom, S.M., Fox, C.R., Trepel, C. & Poldrack, R.A. The neural basis of loss aversion in decision-making under risk. *Science* **315**, 515-518 (2007).
13. Wallis, J.D. Cross-species studies of orbitofrontal cortex and value-based decision-making. *Nat Neurosci* **15**, 13-19 (2011).
14. Roesch, M.R. & Olson, C.R. Neuronal activity related to reward value and motivation in primate frontal cortex. *Science* **304**, 307-310 (2004).
15. Wunderlich, K., Rangel, A. & O'Doherty, J.P. Neural computations underlying action-based decision making in the human brain. *Proc Natl Acad Sci U S A* **106**, 17199-17204 (2009).
16. O'Doherty, J.P. The problem with value. *Neurosci Biobehav Rev* **43**, 259-268 (2014).
17. Litt, A., Plassmann, H., Shiv, B. & Rangel, A. Dissociating valuation and saliency signals during decision-making. *Cereb Cortex* **21**, 95-102 (2011).
18. Wang, X.J. Decision making in recurrent neuronal circuits. *Neuron* **60**, 215-234 (2008).
19. Casey, B.J.*, et al.* The Adolescent Brain Cognitive Development (ABCD) study: Imaging acquisition across 21 sites. *Dev Cogn Neurosci* **32**, 43-54 (2018).
20. Krebs, R.M., Heipertz, D., Schuetze, H. & Duzel, E. Novelty increases the mesolimbic functional connectivity of the substantia nigra/ventral tegmental area (SN/VTA) during reward anticipation: Evidence from high-resolution fMRI. *NeuroImage* **58**, 647-655 (2011).
21. Ferenczi, E.A.*, et al.* Prefrontal cortical regulation of brainwide circuit dynamics and reward-related behavior. *Science* **351**, aac9698 (2016).
22. Lutz, K. & Widmer, M. What can the monetary incentive delay task tell us about the neural processing of reward and punishment? *Neuroscience and Neuroeconomics* (2014).

23. Lake, J.I., *et al.* Reward anticipation and punishment anticipation are instantiated in the brain via opponent mechanisms. *Psychophysiology* **56**, e13381 (2019).
24. Van Essen, D.C., *et al.* The Human Connectome Project: a data acquisition perspective. *Neuroimage* **62**, 2222-2231 (2012).
25. Arulpragasam, A.R., Cooper, J.A., Nuutinen, M.R. & Treadway, M.T. Corticoinsular circuits encode subjective value expectation and violation for effortful goal-directed behavior. *Proc Natl Acad Sci U S A* **115**, E5233-E5242 (2018).
26. Botvinick, M.M., Braver, T.S., Barch, D.M., Carter, C.S. & Cohen, J.D. Conflict monitoring and cognitive control. *Psychol Rev* **108**, 624-652 (2001).
27. Mumford, J.A., *et al.* Detecting network modules in fMRI time series: a weighted network analysis approach. *Neuroimage* **52**, 1465-1476 (2010).
28. Combes, S., *et al.* Relationships between sensory and physicochemical measurements in meat of rabbit from three different breeding systems using canonical correlation analysis. *Meat Sci* **80**, 835-841 (2008).
29. Winkler, A.M., Renaud, O., Smith, S.M. & Nichols, T.E. Permutation inference for canonical correlation analysis. *Neuroimage* **220**, 117065 (2020).
30. Matsumoto, H., Tian, J., Uchida, N. & Watabe-Uchida, M. Midbrain dopamine neurons signal aversion in a reward-context-dependent manner. *Elife* **5** (2016).
31. Monosov, I.E., Leopold, D.A. & Hikosaka, O. Neurons in the Primate Medial Basal Forebrain Signal Combined Information about Reward Uncertainty, Value, and Punishment Anticipation. *J Neurosci* **35**, 7443-7459 (2015).
32. Cohen, J.Y., Haesler, S., Vong, L., Lowell, B.B. & Uchida, N. Neuron-type-specific signals for reward and punishment in the ventral tegmental area. *Nature* **482**, 85-88 (2012).
33. de Jong, J.W., *et al.* A Neural Circuit Mechanism for Encoding Aversive Stimuli in the Mesolimbic Dopamine System. *Neuron* **101**, 133-151 e137 (2019).
34. Fiorillo, C.D. Two dimensions of value: dopamine neurons represent reward but not aversiveness. *Science* **341**, 546-549 (2013).
35. Cauda, F., *et al.* Functional connectivity and coactivation of the nucleus accumbens: a combined functional connectivity and structure-based meta-analysis. *J Cogn Neurosci* **23**, 2864-2877 (2011).
36. Hiser, J. & Koenigs, M. The Multifaceted Role of the Ventromedial Prefrontal Cortex in Emotion, Decision Making, Social Cognition, and Psychopathology. *Biol Psychiatry* **83**, 638-647 (2018).
37. Levy, D.J. & Glimcher, P.W. The root of all value: a neural common currency for choice. *Curr Opin Neurobiol* **22**, 1027-1038 (2012).
38. Haber, S.N. & Knutson, B. The reward circuit: linking primate anatomy and human imaging. *Neuropsychopharmacology* **35**, 4-26 (2010).
39. Knutson, B., Westdorp, A., Kaiser, E. & Hommer, D. FMRI Visualization of Brain Activity during a Monetary Incentive Delay Task. *NeuroImage* **12**, 20-27 (2000).
40. Rolls, E.T., Huang, C.C., Lin, C.P., Feng, J. & Joliot, M. Automated anatomical labelling atlas 3. *Neuroimage* **206**, 116189 (2020).
41. Langfelder, P. & Horvath, S. WGCNA: an R package for weighted correlation network analysis. *BMC Bioinformatics* **9**, 559 (2008).
42. Jia, T., *et al.* Neurobehavioural characterisation and stratification of reinforcement-related behaviour. *Nat Hum Behav* **4**, 544-558 (2020).

Figures:

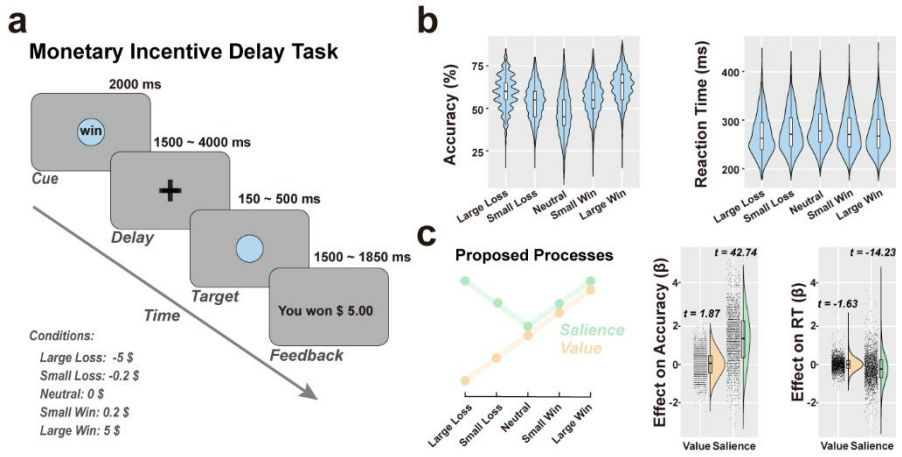

Figure 1. Experimental design and task performances. a. The procedure of the monetary incentive delay task (MID); **b.** Distributions of task performance in different conditions; **c.** Proposed value and salience processes and their impacts on task performances.

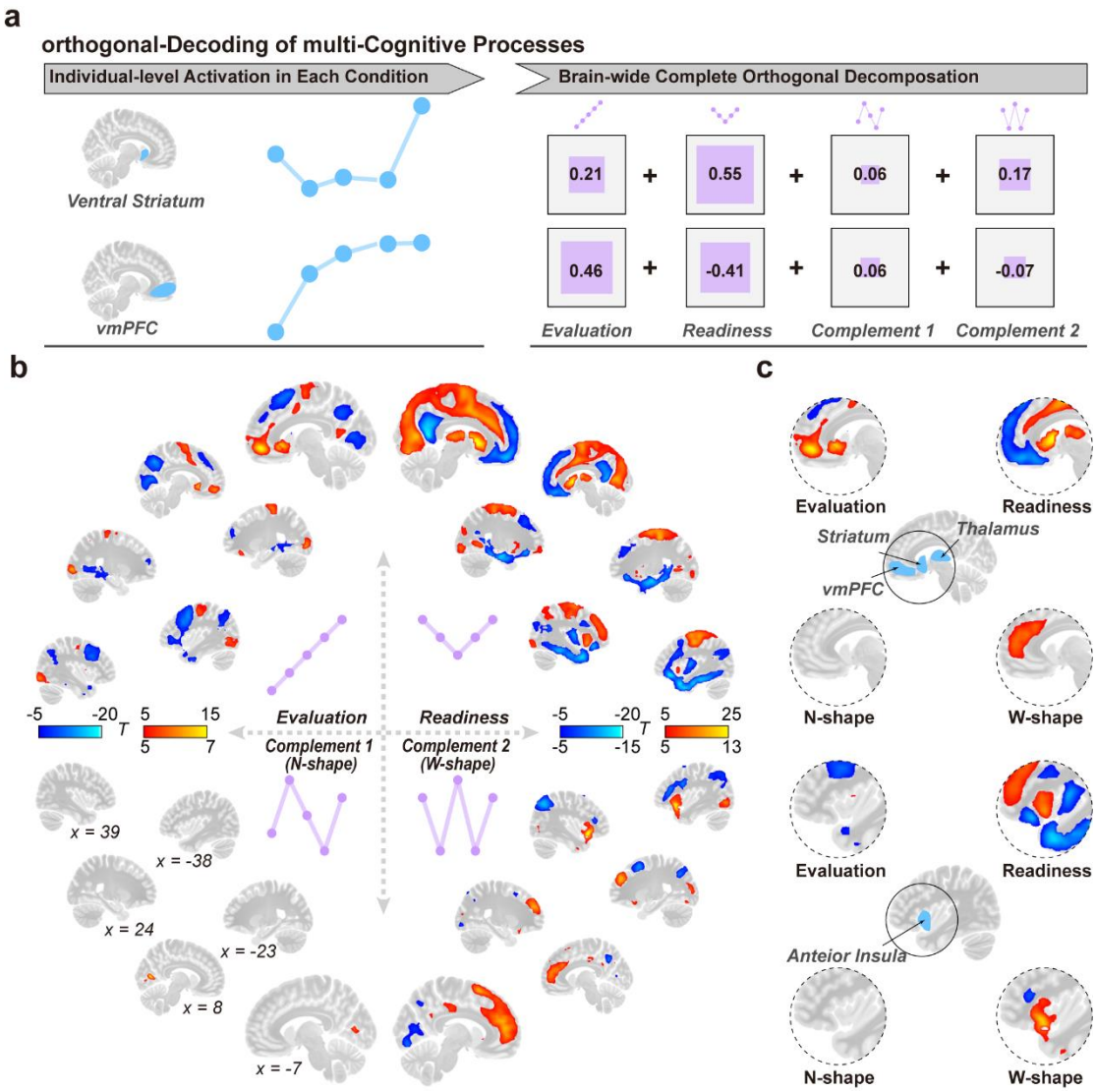

Figure 2. Neural representations of the orthogonal decomposition. a. An illustration of the Orthogonally Decoding of multi-Cognitive Process (DeCoP); **b.** Brain-wide T-maps of decomposed signals for orthogonal contrasts. Brain-wide significance was set as $|T|>5$. The MNI coordinates of brain slices were shown at the lower left; **c.** Decomposed signals in key brain regions.

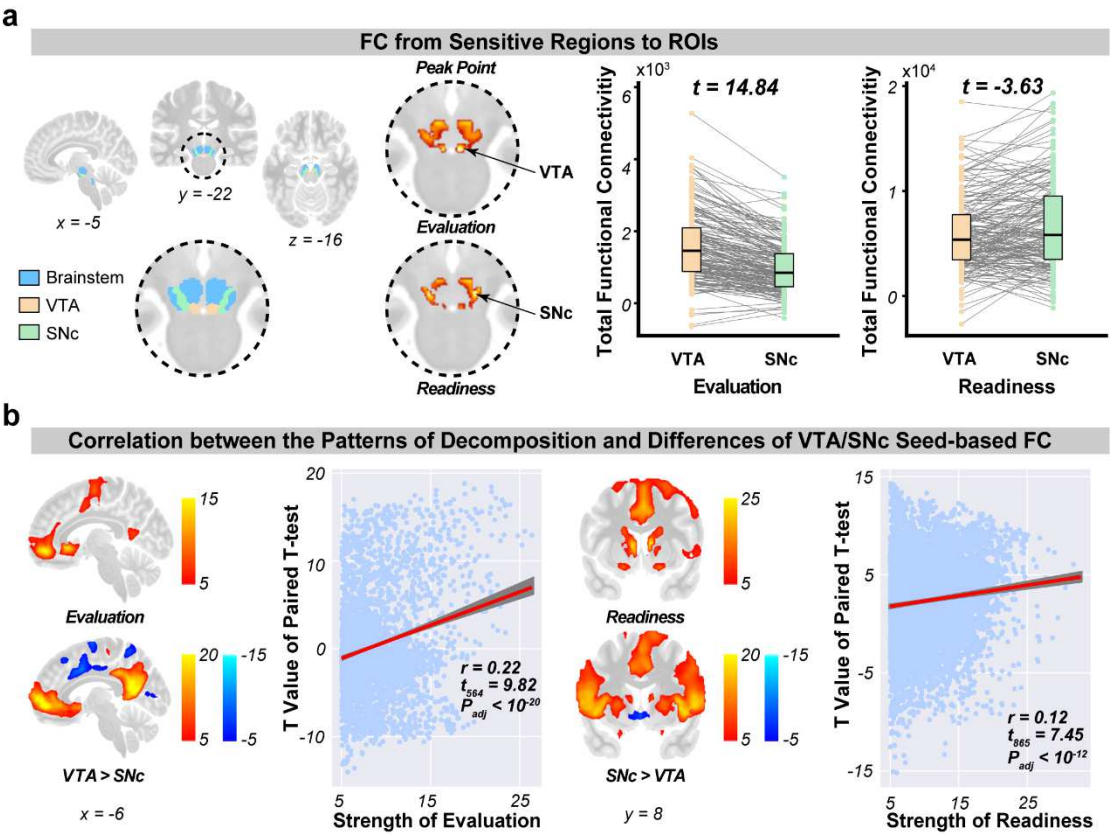

Figure 3. Decomposed evaluation and readiness processes target VTA and SNc neural circuits respectively. a. Left: the masks of Brainstem, VTA and SNc from AAL3 atlas; Middle: the strength of functional connectivity (FC) to VTA and SNc from the evaluation and readiness regions identified in Fig. 2B; Right: Paired t-tests between FCs to VTA and SNc from evaluation and readiness; **b.** Brain-wide pattern correlations between the strength of decomposition signals (left: evaluation; right: readiness) and the differenciation of seed-based FCs from VTA and SNc. Brain-wide significance was set as |T|>5.

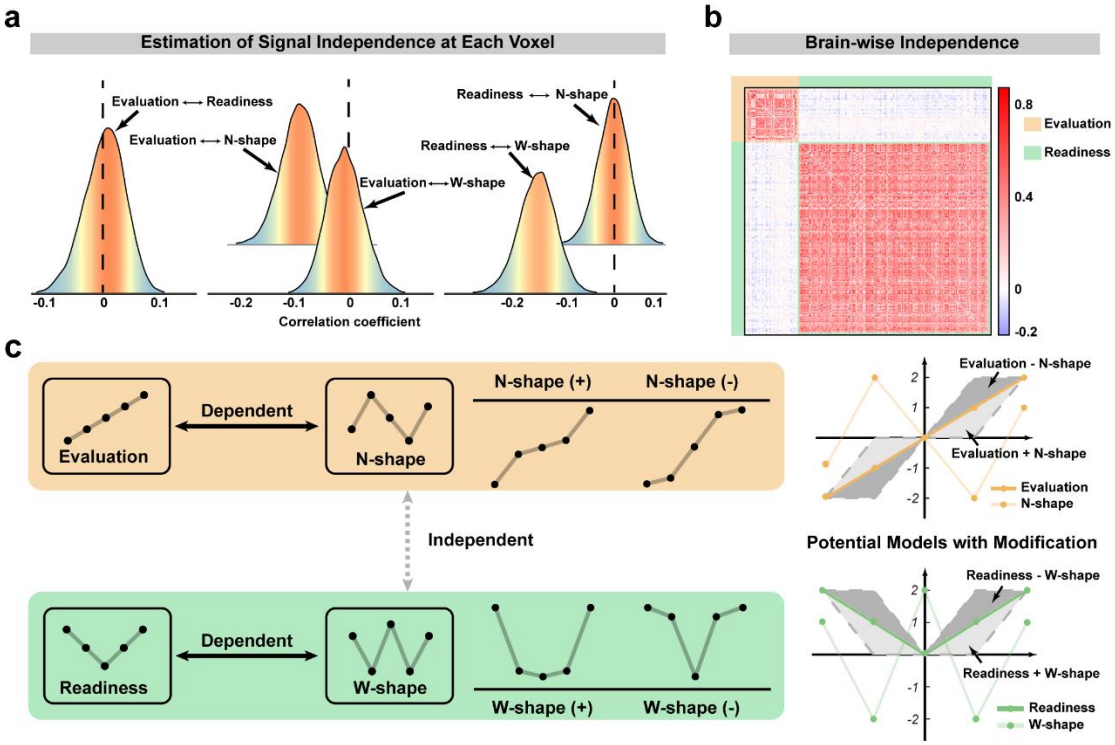

Figure 4. Inference for independence among orthogonally decomposed signals during reward anticipation. a. Distributions of pair-wise correlations between signals of orthogonal contrasts at each voxel, where mean correlations deviated from 0 indicate related signals; **b.** The correlation matrix of signals from the evaluation and readiness clusters identified by WVCNA; **c.** An illustration of how related signals could describe the evaluation-related and readiness-related processing.

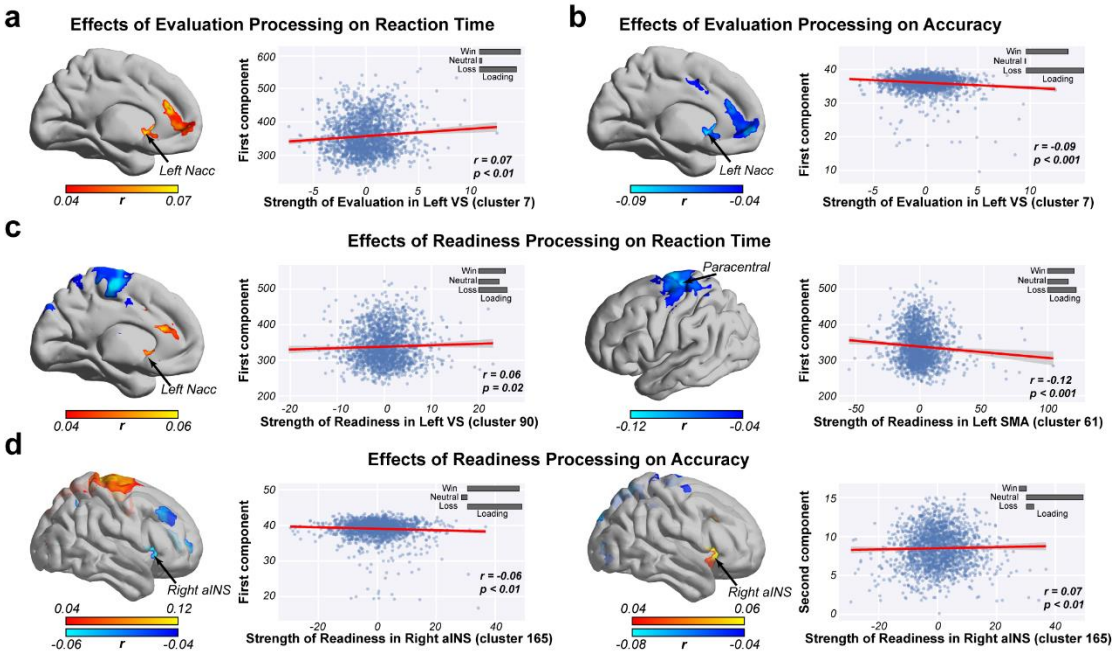

Figure 5. Impacts of evaluation and readiness processing on task performance. The canonical correlation analysis (CCA) was implemented to further segregate signal components that demonstrated differential associations with task performance under different experimental conditions (a-d). The loadings of behavioural components (i.e. of reaction time or accuracy) are shown in the upper right corner of the subgraphs. The black arrow points to the most significant cluster. Also see Extended Data Table 5-6.

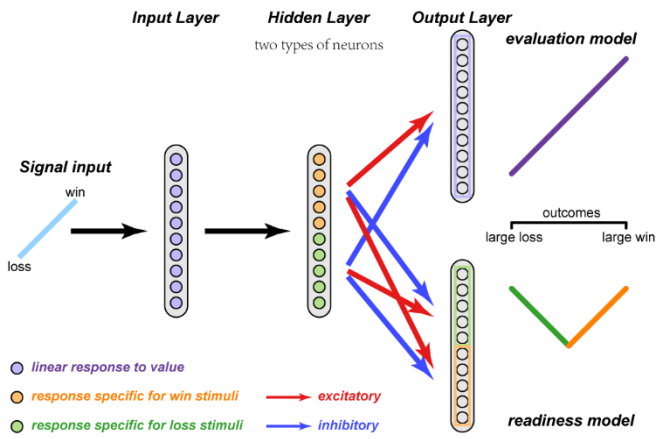

Figure 6. An illustration of the theoretical neuronal encoding model. Although trained individually, both neural networks (i.e. for evaluation and readiness outputs respectively) only differ at the output layer. They hence form an integrated neural network that could decompose the same input (i.e. a value input) into two distinct outputs (i.e. evaluation vs readiness models). Dots represent neurons; red lines represent positive connections, and blue lines represent negative ones. Also see Extended Data Fig. S6.

Extended Data Figures

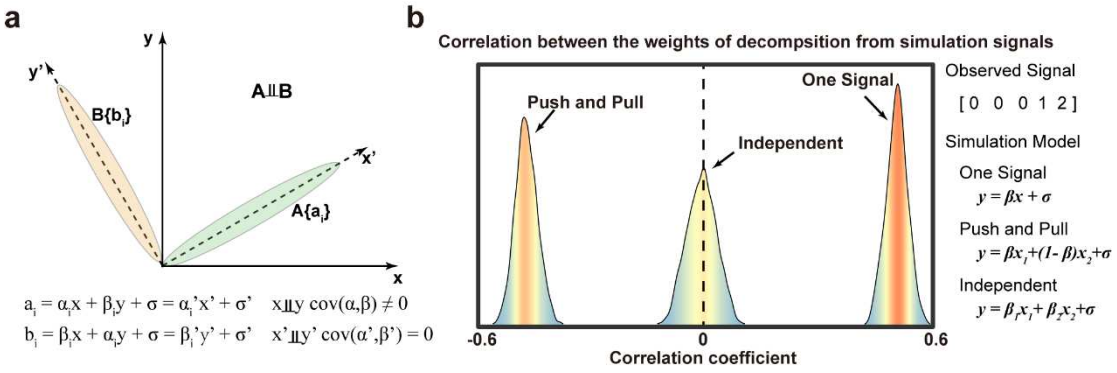

Extended Data Fig. 1. a. Only the "correct" orthogonal vectors could retrieve latent independent signals. **b.** Correlations between decomposed signals based on different simulation models. Also see Extended Data Table 2.

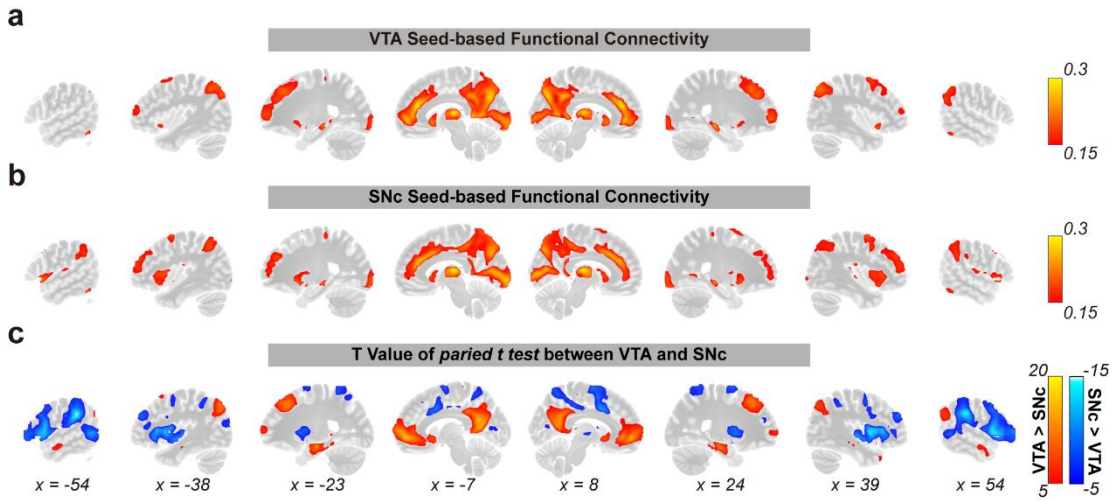

Extended Data Fig. 2. The brain-wide patterns of seed-based functional connectivity (FC) strength from regions of interest (ROIs). a. VTA seed-based FC strength; **b.** SNc seed-based FC strength; **C.** The T-map of differenciated seed-based FC from VTA and SNc.

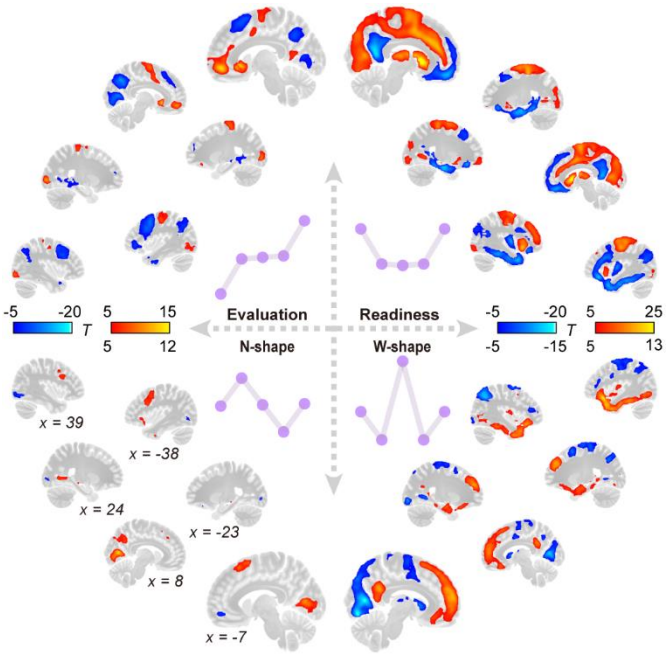

Extended Data Fig. 3. Brain-wide neural representations of signal decomposition with the exact-scale setting (e.g. the evaluation contrast takes the form [-5, -0.2, 0, 0.2, 5] from large-loss to large-win, consistent with the parametric nature of the exact monetary magnitude in the experimental design).

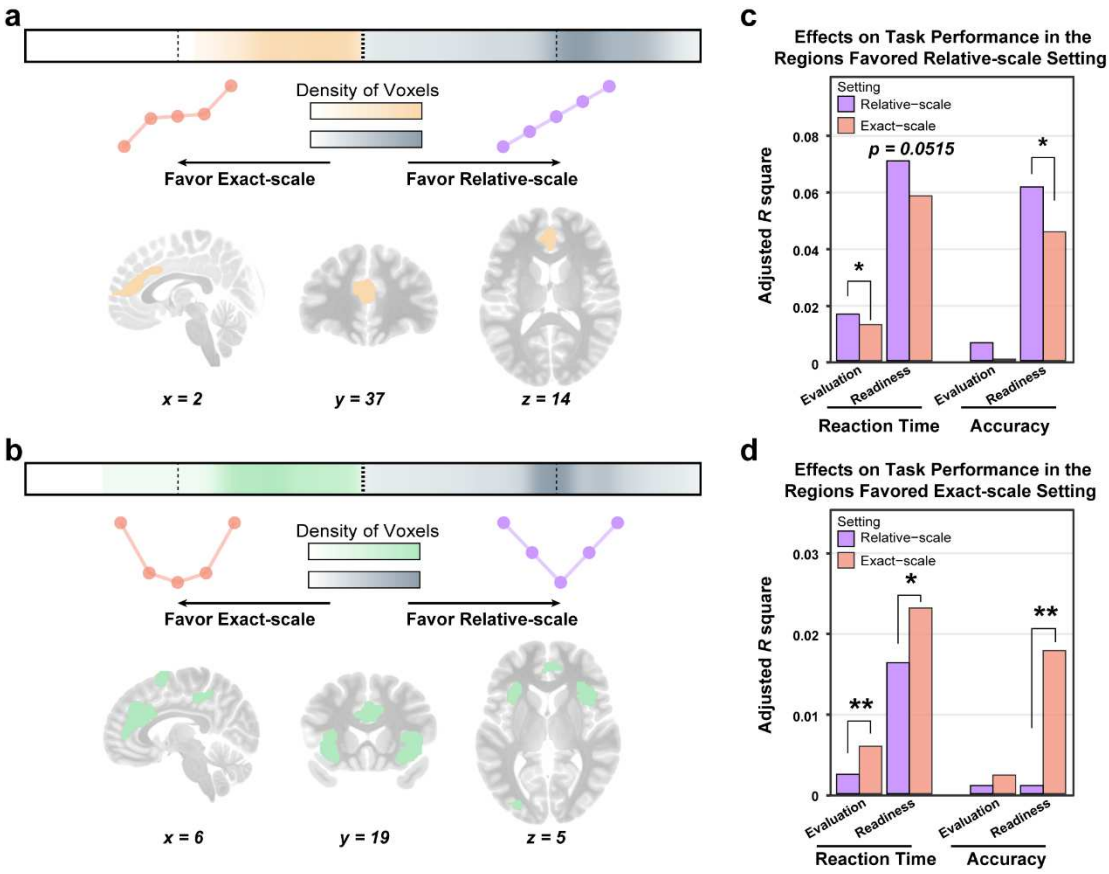

Extended Data Fig. 4. The optimal models for latent neurobehavioural signals. The bimodal distribution of voxels favoring the exact-scale or relative-scale settings in evaluation (a) and readiness (b) processing. The typical regions favoring the exact-scale setting were illustrated in the corresponding lower subplots; (c&d) The favoured neural representations (i.e. relative-scale vs exact-scale) demonstrated better predictions for task performance. *significant at level 0.05, ** significant at level 0.01.

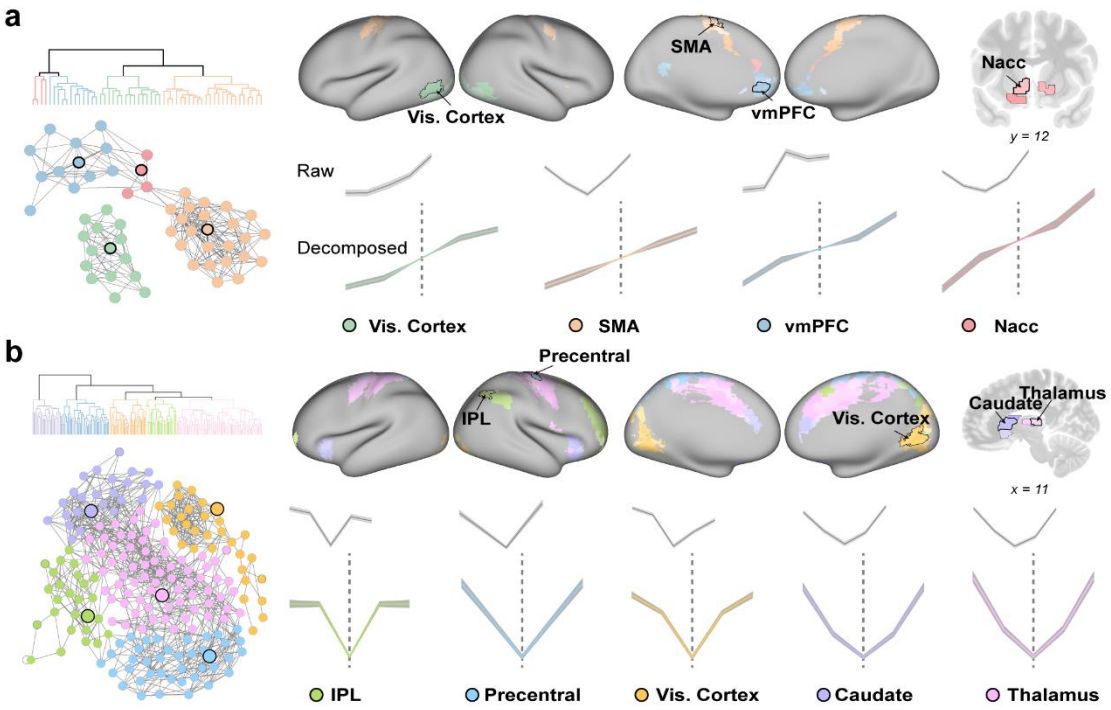

Extended Data Fig. 5. The brain clusters and subnetworks of evaluation **(a)** and readiness **(b)** processing. Also see Extended Data Table 4. The core brain region of each subnetwork is marked by a black bound and illustrated in both the networks (left) and brain templates (right). Raw and decomposed signals of the core brain regions are presented below the brain.

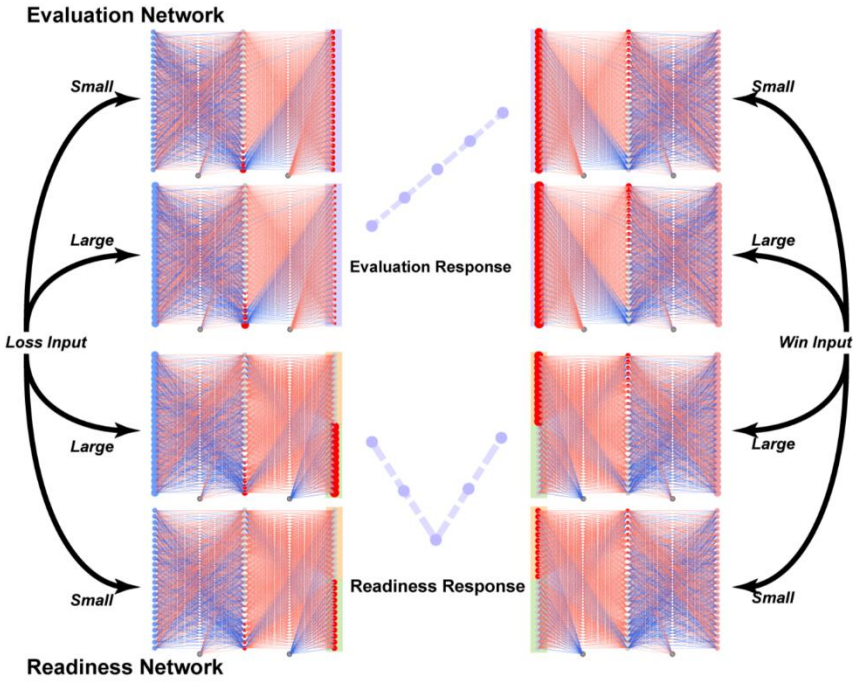

Extended Data Fig. 6. Graphical visualisation of the artificial neural networks. Dots represent neurons; red lines represent positive connections and blue lines represent negative ones. The red dots in the hidden and output layers represent activated neurons. The larger the dot is, the stronger the neuron activates.

Supplementary Files

This is a list of supplementary files associated with this preprint. Click to download.

- ExtendedDataTable16.xlsx
- SupplementaryInformation.pdf